

Ab initio simulation of solid electrolyte materials in liquid and glassy phases

B. Prasai and D. A. Drabold*

Department of Physics and Astronomy, Ohio University, Athens, Ohio 45701, USA

(Received 10 November 2010; revised manuscript received 27 January 2011; published 16 March 2011)

We use plane-wave density functional methods to model Ge-Se-Ag-Cu liquids and glasses. The models are analyzed for structural and electronic properties and transition metal ion dynamics. Electronic properties are analyzed with the electronic density of states and projected density of states. The optical gap increases with increasing Ag content and decreases with increasing Cu content. We carry out thermal simulation at 300, 700, and 1000 K on these Ge-Se glasses doped with various concentrations of copper and silver. Our study shows that the most diffusive ions sample the widest variation in local density. The study of trap centers for Ag-rich and Cu-rich glasses shows that because of the higher coordination number of Cu, it is more rigidly trapped compared to Ag, with its lower coordination number.

DOI: [10.1103/PhysRevB.83.094202](https://doi.org/10.1103/PhysRevB.83.094202)

PACS number(s): 61.43.Dq, 71.23.Cq, 66.30.hh

I. INTRODUCTION

Chalcogenide glasses have been studied extensively for the last few decades, both for their basic scientific interest and because they are preferred materials for applications such as optical recording devices¹ and phase change memory.² There has been particular interest in Ge-Se glasses because of their excellent glass formation characteristics: the $\text{Ge}_x\text{Se}_{1-x}$ binary system is an excellent glass former for $x \leq 0.43$.³ When doped with metals like Ag, Ge-Se glasses become solid electrolytes offering high ionic conductivities. Such electrolytes are getting attention for their technological importance, with the application in “conducting bridge” (flash) memory devices.⁴ Since the properties of chalcogenide glasses accrue from their structure, the knowledge of the structure of these glasses is an essential precursor for further study.

The structure of GeSe glasses has been widely studied, and the basic structural units consist of Ge-Se tetrahedra and Se chains combined in various ways. X-ray⁵ and neutron^{6,7} diffraction and other experimental methods have been used to study the structure of Ge-Se-Ag glass. There have also been some computational studies to model the structure. Tafen *et al.*⁸ reported two *ab initio* models, $(\text{GeSe}_3)_{0.9}\text{Ag}_{0.1}$ and $(\text{GeSe}_3)_{0.85}\text{Ag}_{0.15}$, with short-range order consistent with the experimental results. It has also been reported that Ag atoms prefer to sit at a trapping center which is near the midpoint of a line joining two host atoms (Ge or Se) separated by a distance of between 4.7 and 5.2 Å.⁹

The purpose of this study is to understand the structure of Ge-Se-Ag, Ge-Se-Cu, and Ge-Se-Ag-Cu glasses and the ion dynamics for the single-ion and mixed-ion cases. Section II of the paper briefly describes the method and the technical details of the simulations. Section III is organized into four distinct subsections, with Sec. III A 1 devoted to the structure of the amorphous models and Sec. III A 2 to the structure of the liquid models. Electronic characteristics of both the amorphous and the liquid systems are presented in Sec. III B through the electronic density of states and the projected density of states. Section III C is devoted to the dynamics of the ions at different temperatures, 300, 700, and 1000 K. The character of the ion traps is described in Sec. III D. Finally, we present a brief summary in Sec. IV.

II. METHODS

We used the melt quenching method to generate the systems described in this work.¹⁰ We constructed a cubic supercell, fixing the volume and the number to reproduce the experimental density according to the desired stoichiometry and with the minimum acceptable distance between two atoms set to 2 Å, starting with a random initial configuration. We generated four models: $(\text{GeSe}_3)_{0.9}\text{Ag}_{0.1}$, with 27 Ge atoms, 81 Se atoms, and 12 Ag atoms; $(\text{GeSe}_3)_{0.8}\text{Ag}_{0.2}$, with 24 Ge atoms, 72 Se atoms, and 24 Ag atoms; $(\text{GeSe}_3)_{0.9}\text{Cu}_{0.1}$, with 27 Ge atoms, 81 Se atoms, and 12 Cu atoms; and $(\text{GeSe}_3)_{0.77}\text{Cu}_{0.03}\text{Ag}_{0.2}$, with 23 Ge atoms, 69 Se atoms, 4 Cu atoms, and 24 Ag atoms. These models were annealed and equilibrated for 2.5 ps at 2000 K, well above the melting points. The cells were then cooled to 1000 K over 10 ps and equilibrated at 1000 K for 5 ps. They were then cooled to 300 K over 14 ps. Next these systems were equilibrated at 300 K for more than 50 ps. Finally, these systems were fully relaxed. All of the calculations were carried out under periodic boundary conditions using the Vienna *Ab Initio* Simulation Package (VASP),¹¹ with Vanderbilt Ultra Soft pseudopotentials. VASP is based on density functional theory using a plane wave basis. We used the local density approximation for the exchange correlation energy. These systems were annealed, equilibrated, and cooled using the molecular dynamics (MD) option of VASP, and relaxation is carried out in the conjugate gradient mode.

III. RESULTS AND DISCUSSION**A. Structural properties****1. Structural properties of amorphous Ge-Se-Ag-Cu**

Figure 1 shows the total radial distribution functions (RDFs) and structure factors for our four different models; $g-(\text{GeSe}_3)_{0.9}\text{Ag}_{0.1}$, $g-(\text{GeSe}_3)_{0.8}\text{Ag}_{0.2}$, $g-(\text{GeSe}_3)_{0.9}\text{Cu}_{0.1}$ and $g-(\text{GeSe}_3)_{0.77}\text{Cu}_{0.03}\text{Ag}_{0.2}$. The first peak of the RDF is the contribution from Ge-Se and Se-Se correlations, whereas the second peak is due to Se-Se and Ge-Ag/Cu correlations (Figs. 2 and 3). There is not much variation in the short-range order, that is, nearest-neighbor distance and second-nearest-neighbor distance for the different models. We observed a slight change in the nearest-neighbor distance

TABLE I. Short-range order; nearest-neighbor distance (NN), next-nearest-neighbor distance (NNN), and mean coordination number (CN).

	NN (Å)	NNN (Å)	CN
(GeSe ₃) _{0.9} Ag _{0.1}	2.49	3.75	2.50
(GeSe ₃) _{0.8} Ag _{0.2}	2.51	3.80	2.92
(GeSe ₃) _{0.77} Cu _{0.03} Ag _{0.2}	2.45	3.80	2.9
(GeSe ₃) _{0.9} Cu _{0.1}	2.40	3.83	2.8

for the Ag-rich model and Cu-rich model. The average bond length and the mean coordination numbers are presented in Table I. Table II gives the mean bond lengths for different bonds present in our models. We did not detect Ge-Ge bonds in any of our models as seen previously in g-(GeSe₃)_{0.9}Ag_{0.1}.⁸ We also observed that both Ag and Cu preferred to have Se as a neighbor, with only 16% of Cu/Ag bonded with Ge in our models. These results are very close to the bond lengths measured by Piarristeguy *et al.*⁵ We have not seen any experiments for Cu-Ge-Se systems; however, the Cu-Se correlation length we observed is not very far from the value (2.42–2.44 Å) measured by Merino *et al.*¹² for CuInSe₂. We also obtained the silver and copper coordination number for each model. The coordination number 3.1 of silver at 20% is as predicted (3.0) by Mitkova *et al.*¹³ The coordination number 4.67 of copper at 10% is much higher than the 2.16 of silver (found to be 2.0 by Tafen *et al.*)⁸ for the same concentration. Topological information is presented in Table III. We detected a few threefold Ge and three- and fourfold Se that we interpret as structural defects in our models.

We also compared the static structure factors for our models (Fig. 1). There is no significant change with composition in the position of the first two peaks. We observed a weak peak in $S(Q)$ slightly above 1 \AA^{-1} . This peak, which is a precursor to the first sharp diffraction peak, varies as a function of Ag concentration; the peak disappears as the Ag concentration increases, which was also shown by Piarristeguy *et al.*¹⁴ We did not observe any particular correlation contributing to this peak as the partial structure factors (Fig. 4) show that the peak has contributions from all of the partials. We compared partial structure factors for (GeSe₃)_{0.9}Ag_{0.1} and (GeSe₃)_{0.9}Cu_{0.1} and observed the only differences in the correlation of Ag-Ag and Cu-Cu as well as in Se-Ag/Cu.

2. Structural properties of liquid Ge-Se-Ag-Cu

We performed thermal MD simulation of our models at 1000 K for 25 ps to obtain well-equilibrated liquid systems. We calculated the RDFs and present them in Fig. 5. The RDFs are

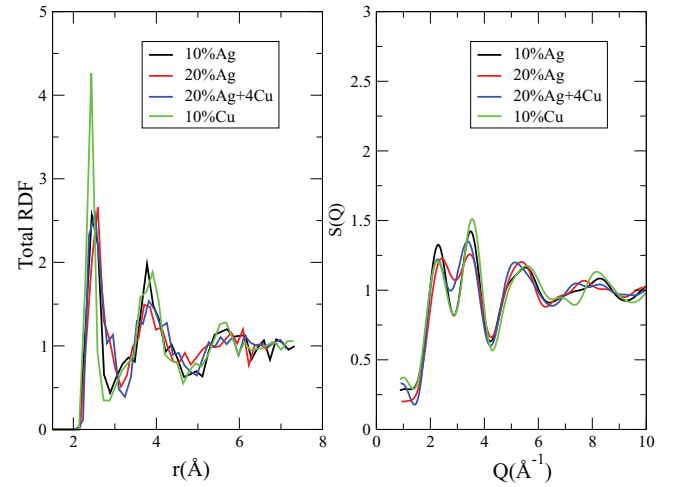


FIG. 1. (Color online) Comparison of total radial distribution functions and static structure factors for all amorphous models.

averaged over the last 2.5 ps. Figure 5 shows the dependence of peak position on the concentration of Ag/Cu, with 2.45 Å for (GeSe₃)_{0.9}Cu_{0.1}, 2.48 Å for (GeSe₃)_{0.9}Ag_{0.1}, and 2.53 Å for (GeSe₃)_{0.8}Ag_{0.2}, and (GeSe₃)_{0.77}Cu_{0.03}Ag_{0.2}. We also present partial RDFs in Fig. 6, showing Ge-Ge, Ge-Se, Se-Se, and Se-Ag/Cu correlations. All of our models except (GeSe₃)_{0.9}Ag_{0.1} (2.6 Å) imply the presence of Ge-Ge homopolar bonds with a peak position at 2.71 Å, in contrast with the glass. We also observed Se-Se and Ge-Se bond distances of 2.47 and 2.50 Å, respectively. We observe no concentration dependence on the first peak position of Ge-Se, Se-Se, and Se-Ag/Cu correlations. The major contribution to the first peak of the total RDF is from Ge-Se, Se-Se, and Se-Ag/Cu correlations, with the Se-Ag/Cu correlation causing the shifts in the first peak positions. The second peak of the total RDF is mainly due to Se-Se correlation. We measured the first peak positions of $g_{\alpha\beta}(r)$ and present them in Table IV.

B. Electronic properties

1. Electronic properties of amorphous Ge-Se-Ag-Cu

We analyzed the electronic structure of our models through electronic density of states (EDOS). Figures 7–10 shows the EDOS and the projected density of states (PDOS) for the different models. The figures show both the species projected DOS and the orbital projected DOS for our systems. The Fermi level has been shifted to $E = 0$ in all cases. From our observation, it can be seen that the basic spectra for our systems look similar to the EDOS of GeSe binary systems.¹⁵

TABLE II. Mean nearest-neighbor bond lengths (Å) in (GeSe₃)_{0.9}Ag_{0.1}, (GeSe₃)_{0.8}Ag_{0.2}, (GeSe₃)_{0.9}Cu_{0.1}, and (GeSe₃)_{0.77}Cu_{0.03}Ag_{0.2} glasses.

	Ge-Se	Se-Se	Ge-Ag	Se-Ag	Ag-Ag	Ge-Cu	Se-Cu	Ag-Cu	Cu-Cu
(GeSe ₃) _{0.9} Ag _{0.1}	2.37	2.39	2.55	2.66	3.0				
(GeSe ₃) _{0.8} Ag _{0.2}	2.37	2.40	2.60	2.66	2.88				
(GeSe ₃) _{0.77} Cu _{0.03} Ag _{0.2}	2.35	2.41	2.60	2.64	2.95	2.34	2.34	2.77	
(GeSe ₃) _{0.9} Cu _{0.1}	2.37	2.40	–	–	–	2.35	2.34	–	2.54
Experiment ¹⁴	2.37	2.37	–	2.67	3.05	–			

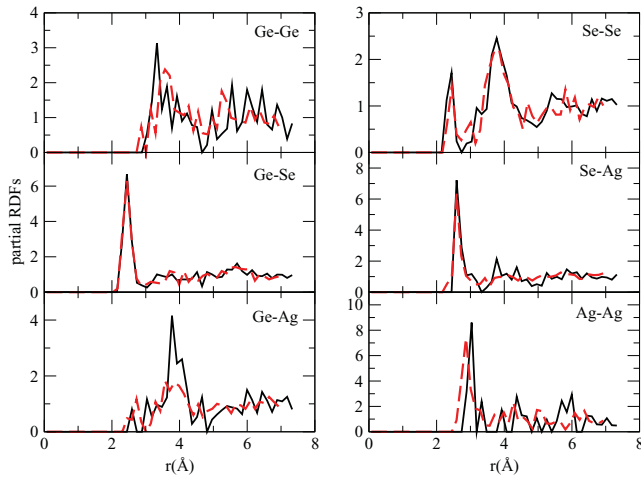


FIG. 2. (Color online) Partial radial distribution functions for amorphous $(\text{GeSe}_3)_{0.9}\text{Ag}_{0.1}$ (black line) and $(\text{GeSe}_3)_{0.8}\text{Ag}_{0.2}$ [dashed (red) line].

For Ag-doped GeSe_3 , the first two bands are dominated by $4s$ -like states of Se and Ge. The third band consists mainly of p -like states of Se and d -like states of Ag and partly s -like states of Ge. The fourth band, that is, the lowest conduction band, contains p -like states of Se and partly s -like states of Ge and d -like states of Ag. The spectrum with the Cu-doped GeSe_3 is also similar to the Ag-doped system, with the Cu contribution mostly to the third band, with its $2d$ -like states at about -2.5 eV. From our simulation we found that the Γ -point optical gap closes as we proceed from Ag-rich to Cu-rich. The narrowing of the gap with the addition of Cu is as predicted by Simdyankin *et al.*¹⁶ and Aniya *et al.*,¹⁷ who showed that for a low concentration of Cu the gap closes with the addition of Cu to AsS and AsSe glasses.

To understand the spatial structure of electron states, we visualize the charge density associated with the eigenstates near the Fermi level. We chose the highest state of the valence band and the lowest state of the conduction band and present the charge density associated with these states in Figs. 11 and 12,

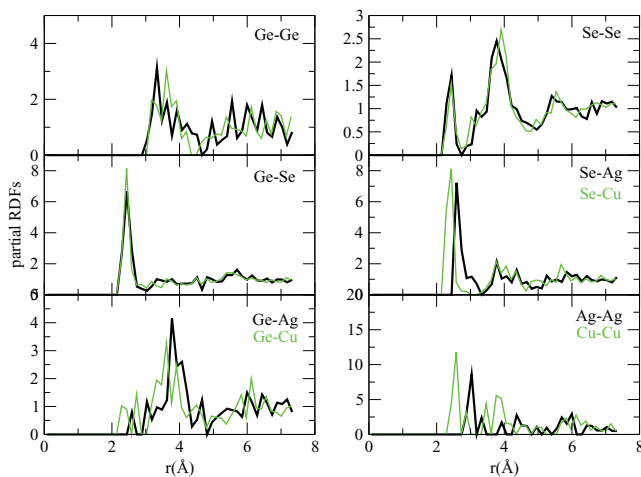


FIG. 3. (Color online) Partial radial distribution functions for amorphous $(\text{GeSe}_3)_{0.9}\text{Ag}_{0.1}$ (black line) and $(\text{GeSe}_3)_{0.9}\text{Cu}_{0.1}$ [thin (green) line].

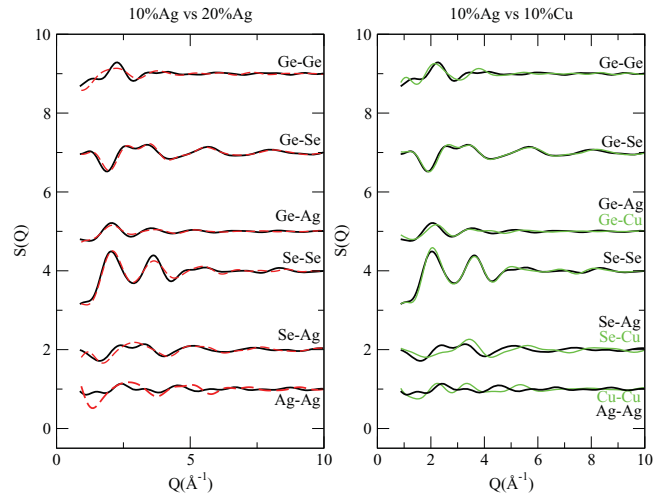


FIG. 4. (Color online) Partial structure factors of amorphous $(\text{GeSe}_3)_{0.9}\text{Ag}_{0.1}$ (black line), $(\text{GeSe}_3)_{0.8}\text{Ag}_{0.2}$ [dashed (red) line] and $(\text{GeSe}_3)_{0.9}\text{Cu}_{0.1}$ [thin (green) line].

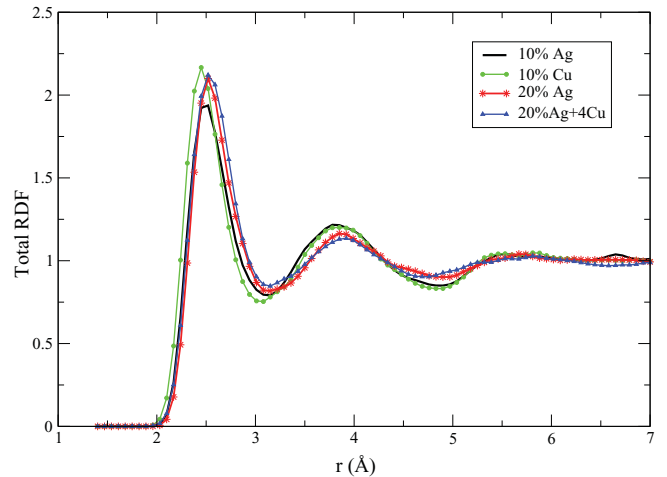


FIG. 5. (Color online) Comparison of total radial distribution functions for all liquid models at 1000 K.

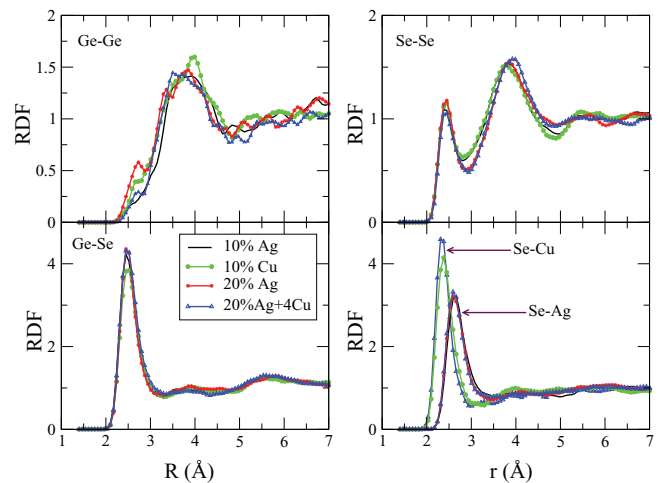


FIG. 6. (Color online) Comparison of partial radial distribution functions for all liquid models at 1000 K.

TABLE III. Coordination statistics for $(\text{GeSe}_3)_{0.9}\text{Ag}_{0.1}$, $(\text{GeSe}_3)_{0.8}\text{Ag}_{0.2}$, $(\text{GeSe}_3)_{0.9}\text{Cu}_{0.1}$, and $(\text{GeSe}_3)_{0.77}\text{Cu}_{0.03}\text{Ag}_{0.2}$ glasses (%).

	Ge		Se			Ag			Cu				
	3-fold	4-fold	2-fold	3-fold	4-fold	2-fold	3-fold	4-fold	2-fold	3-fold	4-fold	5-fold	6-fold
$(\text{GeSe}_3)_{0.9}\text{Ag}_{0.1}$	25.9	55.6	67.9	29.6	–	66.7	25.0	–	–	–	–	–	–
$(\text{GeSe}_3)_{0.8}\text{Ag}_{0.2}$	25.0	75.0	45.8	33.3	15.3	20.8	50.0	29.2	–	–	–	–	–
$(\text{GeSe}_3)_{0.77}\text{Cu}_{0.03}\text{Ag}_{0.2}$	8.7	73.9	39.1	39.1	11.6	12.5	66.7	20.8	25.0	25.0	50.0	–	–
$(\text{GeSe}_3)_{0.9}\text{Cu}_{0.1}$	18.5	70.5	63.0	27.2	3.7	–	–	–	–	–	41.7	50.0	8.3

respectively. Figure 12 illustrates a somewhat localized state where the charge is primarily in a small cluster of atoms, whereas Fig. 11 illustrates a less localized state or the linear combination of nearly localized states where the charge is distributed to a big cluster. It should be stated that these states are not fully localized in an Anderson sense but are strongly spatially nonuniform near the band edge.¹⁰ Furthermore, these figures clearly illustrate the dominance of p -like Se states and d -like Ag states on the valence tail and p -like Se states on the conduction tail.

We also analyzed the contribution of each species to the total EDOS near the gap region. Ge does not contribute to the EDOS near the Fermi level in any of our models. But when we look at the contribution of Se, we see substantial changes in our models near the gap region. To understand this we projected the Se EDOS as a function of its coordination number but we did not observe any correlations. However, when we analyzed the Se EDOS for Se bonded with Cu or Ag and Se not bonded with Cu or Ag, we observed some differences as shown in Fig. 13. Independent of the coordination number, Se bonded with Ag opens the gap, whereas Se bonded with Cu closes the gap. Cu also makes a contribution to the total EDOS in the gap region, however, it is lower than that of Se in that region.

2. Electronic properties of liquid Ge-Se-Ag-Cu

To explore electronic properties of the liquid systems we calculated the electronic density of states at 1000 K. We observed qualitatively similar pictures of the EDOS for all the models. To illustrate, we present the EDOS of liquid $(\text{GeSe}_3)_{0.8}\text{Ag}_{0.2}$ along with that of amorphous $(\text{GeSe}_3)_{0.8}\text{Ag}_{0.2}$ in Fig. 14. Relative to the glass, we observed almost no change in valence band, in contrast to the conduction band, which has been shifted toward the valence band, filling the gap completely. The presence of a few homopolar Ge-Ge bonds, twofold Ge (25%), onefold Se (18%), and onefold Ag (13%), compared to none of these observed in amorphous $(\text{GeSe}_3)_{0.8}\text{Ag}_{0.2}$, is also noted.

TABLE IV. Mean nearest-neighbor bond lengths (Å) in $(\text{GeSe}_3)_{0.9}\text{Ag}_{0.1}$, $(\text{GeSe}_3)_{0.8}\text{Ag}_{0.2}$, $(\text{GeSe}_3)_{0.9}\text{Cu}_{0.1}$, and $(\text{GeSe}_3)_{0.77}\text{Cu}_{0.03}\text{Ag}_{0.2}$ liquids at 1000 K.

	Ge-Ge	Ge-Se	Se-Se	Ge-Ag	Se-Ag	Ag-Ag	Ge-Cu	Se-Cu	Ag-Cu	Cu-Cu
$(\text{GeSe}_3)_{0.9}\text{Ag}_{0.1}$	2.6	2.50	2.47	3.0	2.60	2.9	–	–	–	–
$(\text{GeSe}_3)_{0.8}\text{Ag}_{0.2}$	2.71	2.50	2.47	2.7	2.60	2.9	–	–	–	–
$(\text{GeSe}_3)_{0.77}\text{Cu}_{0.03}\text{Ag}_{0.2}$	2.71	2.50	2.47	2.7	2.60	2.9	2.46	2.31	2.80	2.67
$(\text{GeSe}_3)_{0.9}\text{Cu}_{0.1}$	2.71	2.50	2.47	–	–	–	2.40	2.35	–	2.60

C. Ion dynamics

We studied the dynamics of Ag and Cu ions in the GeSe_3 host by computing the mean square displacement for each atomic constituent as

$$\langle r^2(t) \rangle_a = \frac{1}{N_a} \sum_{i=1}^{N_a} \langle |\vec{r}_i(t) - \vec{r}_i(0)|^2 \rangle, \quad (1)$$

where the quantity within the angle braces is the calculated statistical average over the particular atomic species α . We carried out constant-temperature MD calculations at three different temperatures, 300, 700, and 1000 K, to study ion dynamics in the amorphous as well as the liquid systems.

1. Amorphous Ge-Se-Cu-Ag

As expected, at 300 K none of the ions showed substantial diffusion. To illustrate the diffusion we chose $T = 700$ K and present the mean square displacement for each species for each system calculated at this temperature in Fig. 15. At 700 K Ag ions show significant diffusion, consistent with the previous result,⁸ in contrast to Cu ions, which do not diffuse as much. To elucidate the diffusion of these ions we examine the trajectories for 20 ps. Figures 16 and 17 show two-dimensional projections of the trajectories of the most and the least diffusive ions in $(\text{GeSe}_3)_{0.9}\text{Ag}_{0.1}$ and $(\text{GeSe}_3)_{0.9}\text{Cu}_{0.1}$. The trajectories illustrate the wide range of diffusion for the ions, with displacement ranging from 1 to 3.87 Å in $(\text{GeSe}_3)_{0.9}\text{Ag}_{0.1}$, 2 to 6.71 Å in $(\text{GeSe}_3)_{0.8}\text{Ag}_{0.2}$, and 1–3.74 Å in $(\text{GeSe}_3)_{0.9}\text{Cu}_{0.1}$. For the mixed-ion model $(\text{GeSe}_3)_{0.77}\text{Cu}_{0.03}\text{Ag}_{0.2}$, this displacement ranges between 1.73 and 2.82 Å for Cu and between 1.41 and 8.06 Å for Ag. For Ag-rich models more than 60% of the ions have displacements greater than the average displacement [2.36 Å in $(\text{GeSe}_3)_{0.9}\text{Ag}_{0.1}$ and 4.47 Å in $(\text{GeSe}_3)_{0.8}\text{Ag}_{0.2}$], whereas for Cu, the majority has displacement smaller than the average (2.11 Å). The wide range of diffusion can be attributed to variation in the local environment of the ions. To illustrate this we calculated the local densities of the most and the least mobile ions in the course of the simulation. We employed a

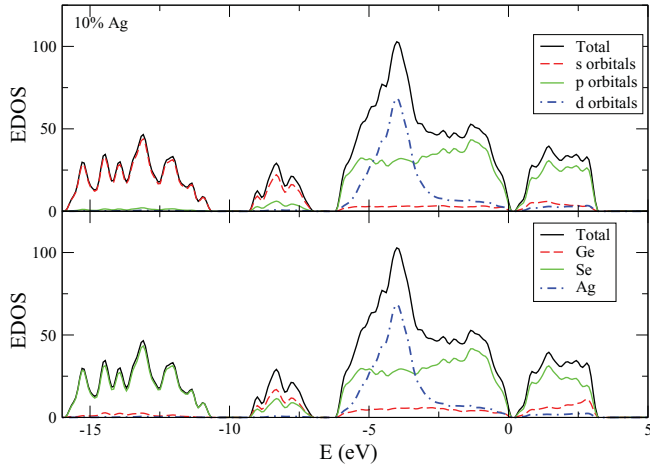


FIG. 7. (Color online) Electronic density of states (EDOS) for amorphous $(\text{GeSe}_3)_{0.9}\text{Ag}_{0.1}$.

sphere of radius 5.0 \AA around the ion and calculated the mean density of atoms inside the sphere. We observed that the most diffusive ion is located in the region with a lower local density. In other words, the most mobile ions have a wider variation of the local density compared to that of the least mobile ion. Figure 18 shows one such comparison.

2. Liquid Ge-Se-Cu-Ag

One of the main properties of a liquid is the high diffusivity of atoms in the system. To illustrate this, we calculated the mean square displacements for each species at 1000 K in all of our models. The diffusion plots as presented in Fig. 19 shows that the mean square displacement of each species increases rapidly compared to that at 700 K. We observe Ag diffusion that is still significantly larger than the host particles, however; Ge and Se atoms are also diffusing rapidly. As before, Cu still does not show high diffusion as Ag does compared to the host atoms.

Based on the plots we calculated diffusion coefficients using the Einstein relation.¹⁸ A time scale of about 20 ps for

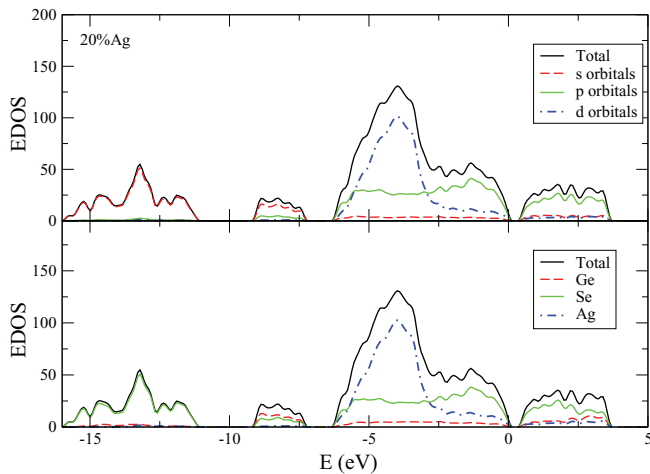


FIG. 8. (Color online) Electronic density of states (EDOS) for amorphous $(\text{GeSe}_3)_{0.8}\text{Ag}_{0.2}$.

TABLE V. Self-diffusion coefficient D and conductivity σ at 300, 700, and 1000 K for $(\text{GeSe}_3)_{0.9}\text{Ag}_{0.1}$ (10%Ag), $(\text{GeSe}_3)_{0.8}\text{Ag}_{0.2}$ (20%Ag), $(\text{GeSe}_3)_{0.9}\text{Cu}_{0.1}$ (10%Cu), and $(\text{GeSe}_3)_{0.77}\text{Cu}_{0.03}\text{Ag}_{0.2}$ (0.77%Cu).

	T (K)	D (cm^2/s)	σ (S cm^{-1})	
			This work	Expt. ¹⁹
10% Ag	300	1.15×10^{-9}	2.63×10^{-5}	1.3×10^{-5}
	700	4.53×10^{-6}	0.0444	0.0207
	1000	1.23×10^{-5}	0.00845	0.0898
20% Ag	300	1.16×10^{-8}	5.3×10^{-4}	7.5×10^{-5}
	700	1.20×10^{-5}	0.235	0.0657
	1000	2.53×10^{-5}	0.347	0.2584
10% Cu	300	7.3×10^{-10}	1.67×10^{-5}	
	700	3.3×10^{-6}	0.0323	
	1000	1.13×10^{-5}	0.0775	
0.77% Cu	300	$D_{\text{Ag}} = 1.06 \times 10^{-8}$	4.85×10^{-4}	
		$D_{\text{Cu}} = 7.16 \times 10^{-9}$	1.63×10^{-5}	
	700	$D_{\text{Ag}} = 1.30 \times 10^{-5}$	0.254	
		$D_{\text{Cu}} = 1.16 \times 10^{-6}$	0.0038	
	1000	$D_{\text{Ag}} = 2.42 \times 10^{-5}$	0.332	
		$D_{\text{Cu}} = 5.24 \times 10^{-6}$	0.012	

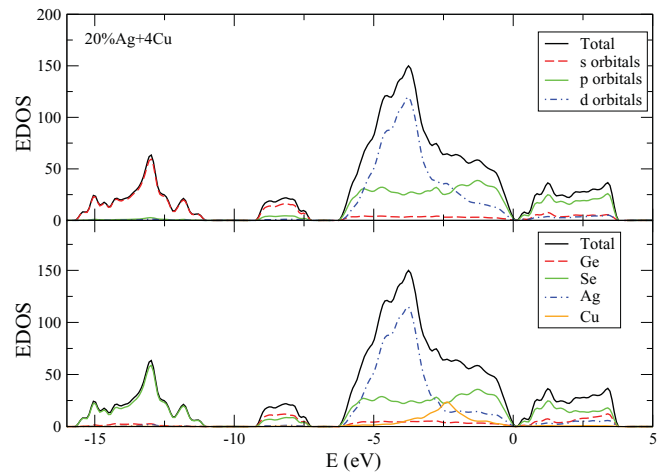


FIG. 9. (Color online) Electronic density of states (EDOS) for amorphous $(\text{GeSe}_3)_{0.77}\text{Cu}_{0.03}\text{Ag}_{0.2}$.

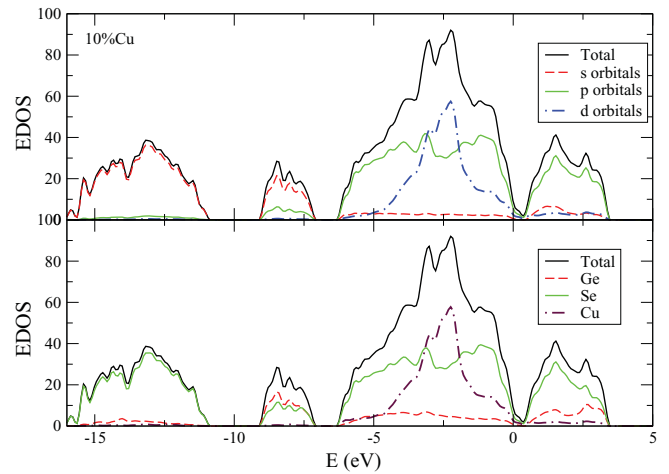


FIG. 10. (Color online) Electronic density of states (EDOS) for amorphous $(\text{GeSe}_3)_{0.9}\text{Cu}_{0.1}$.

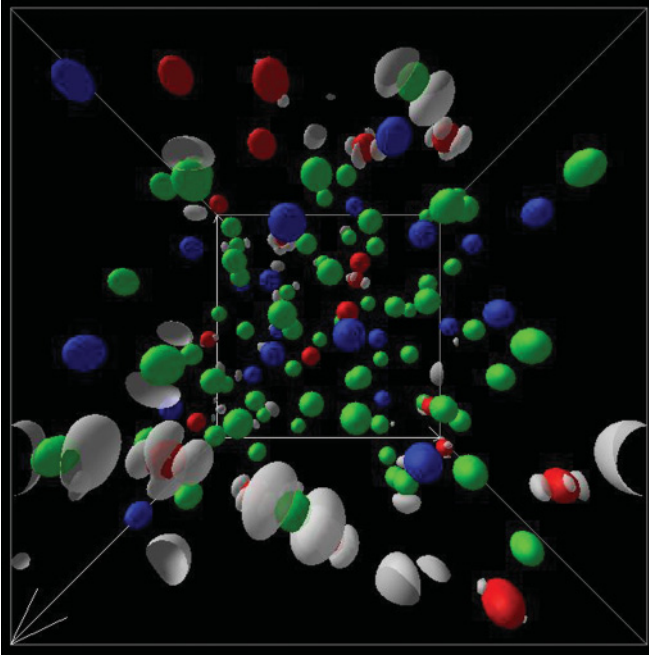


FIG. 11. (Color online) Charge isosurfaces of the highest state of the valence band in amorphous $(\text{GeSe}_3)_{0.8}\text{Ag}_{0.2}$. Blue, green, and red spheres are, respectively, Ge, Se, and Ag atoms, and white clouds around the atoms are the charge density.

our simulation was adequate to equilibrate the systems. The Einstein relation for self-diffusion is given by

$$\langle |\vec{r}_i(t) - \vec{r}_i(0)|^2 \rangle = 6Dt + C, \quad (2)$$

where C is a constant and D is the self-diffusion coefficient. The conductivity can be calculated from the equation

$$\sigma = \frac{ne^2D}{k_B T}, \quad (3)$$

where n is the number density of ions. The temperature dependence of the diffusion is shown in Fig. 20 and the values of diffusion coefficients and conductivities at different temperatures are listed in Table V. We did not find experimental results for the conductivity of Cu ions; however, Ag conductivity is consistent with those reported by Urena *et al.*¹⁹

D. Trap centers and hopping of ions

To illustrate the different ionic transport properties of Ag and Cu, it is essential to study the local environment of Ag and Cu in our models. Figure 21 shows the local environment for Ag and Cu in $(\text{GeSe}_3)_{0.9}\text{Ag}_{0.1}$ and $(\text{GeSe}_3)_{0.9}\text{Cu}_{0.1}$, respectively. In the relaxed networks, most of the Ag ions (58.3%) are found to occupy trap centers between two of the host sites as also predicted by the previous workers,^{8,9} but this is not the case with Cu. Cu is always surrounded by more than two host atoms, which makes the traps for Cu more rigid than for Ag. In Ag-rich systems at 300 K, we observed that Ag is basically trapped, with only a few hopping events. At 700 K the lifetime of the trap decreases and hopping occurs. We observed the lifetime of the traps to vary from 1 to 3.5 ps. However, at 1000 K we failed to observe the well-defined hopping events because of the high diffusion of the host itself.

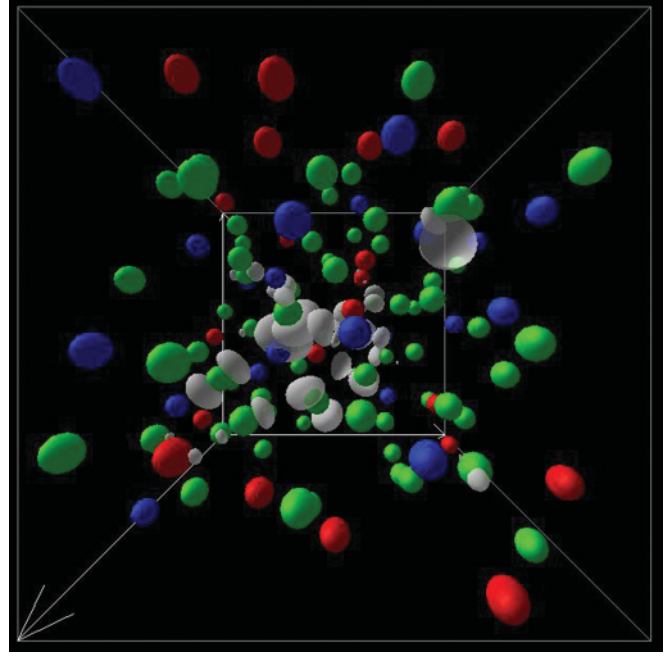


FIG. 12. (Color online) Charge isosurfaces of the lowest state of the conduction band in amorphous $(\text{GeSe}_3)_{0.8}\text{Ag}_{0.2}$. Blue, green, and red spheres are, respectively, Ge, Se, and Ag atoms, and white clouds around the atoms are the charge density.

In the Cu-rich system the story is completely different. Even at 700 K we could observe only a few hopping events with a much longer trap lifetime. It has also been shown by previous workers that the nature of a trap or cage depends mainly on the coordination number, nearest-neighbor distance, and angular distribution of the nearest neighbors.²⁰ The low coordination number of Ag makes it easy to escape the trap, whereas for Cu its high coordination number, smaller neighbor distance, and uniform angular distribution like a tetrahedral network make it very hard to escape from the trap.

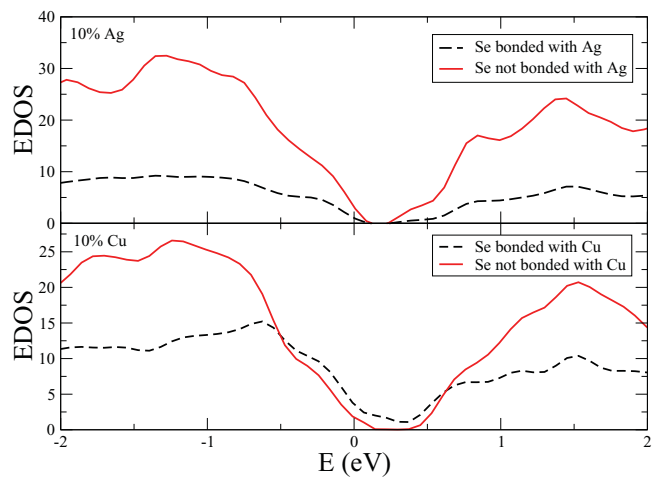


FIG. 13. (Color online) Comparison of Se projected electronic density of states between Se bonded with Ag/Cu and Se not bonded with Ag/Cu in amorphous $(\text{GeSe}_3)_{0.9}\text{Ag}_{0.1}$ and $(\text{GeSe}_3)_{0.9}\text{Cu}_{0.1}$.

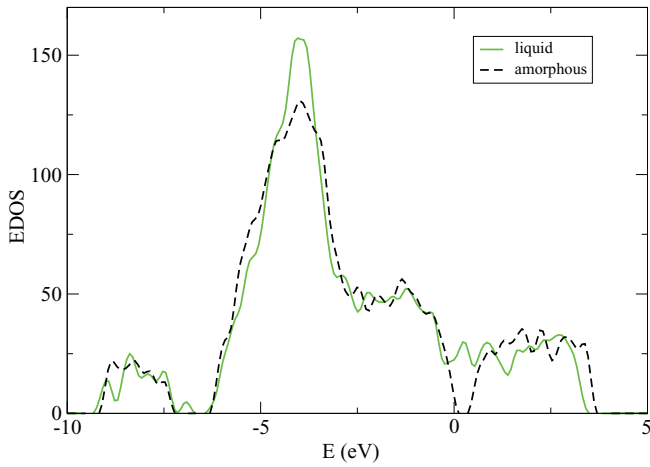


FIG. 14. (Color online) Electronic density of states (EDOS) for liquid $(\text{GeSe}_3)_{0.8}\text{Ag}_{0.2}$ [solid (green) line] and amorphous [dashed (black) line] $(\text{GeSe}_3)_{0.8}\text{Ag}_{0.2}$. Fermi level shifted to 0 eV.

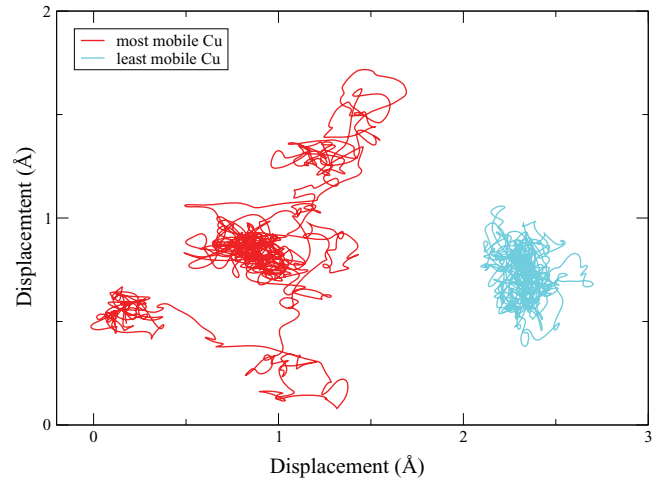


FIG. 17. (Color online) Trajectories of the most and the least diffusive Cu ions at 700 K as a function of time in amorphous $(\text{GeSe}_3)_{0.9}\text{Cu}_{0.1}$. Simulation time, 20 ps.

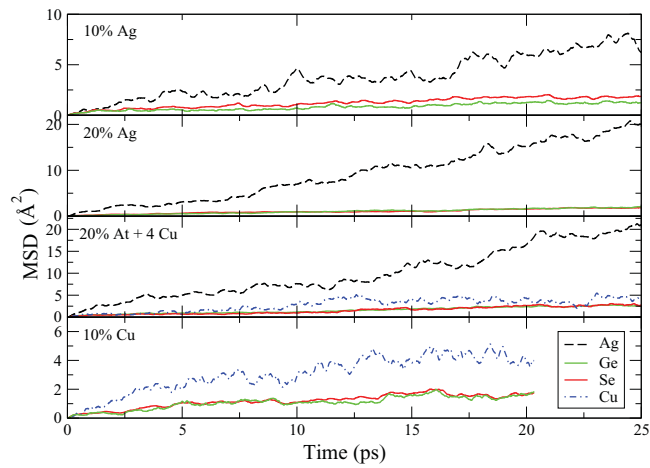


FIG. 15. (Color online) Mean square displacement of atoms in amorphous $(\text{GeSe}_3)_{0.9}\text{Ag}_{0.1}$, $(\text{GeSe}_3)_{0.8}\text{Ag}_{0.2}$, $(\text{GeSe}_3)_{0.77}\text{Cu}_{0.03}\text{Ag}_{0.2}$, and $(\text{GeSe}_3)_{0.9}\text{Cu}_{0.1}$ (top to bottom, respectively) glasses at $T = 700$ K. Ag (black line), Ge (green line), Se (red line), and Cu (blue line).

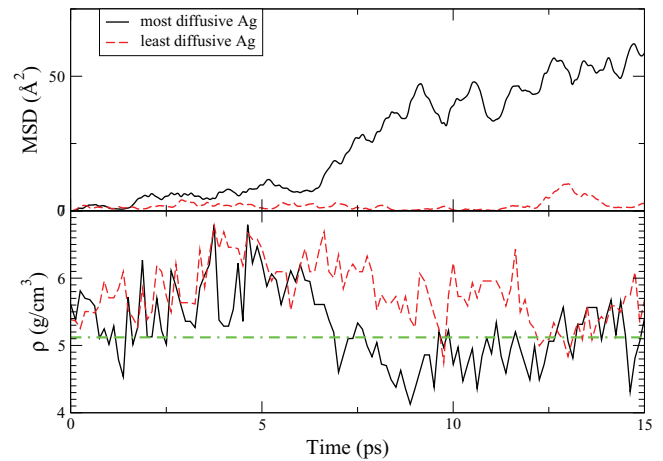


FIG. 18. (Color online) Local density of the most and the least diffusive Ag ions at 700 K as a function of time in amorphous $(\text{GeSe}_3)_{0.8}\text{Ag}_{0.2}$.

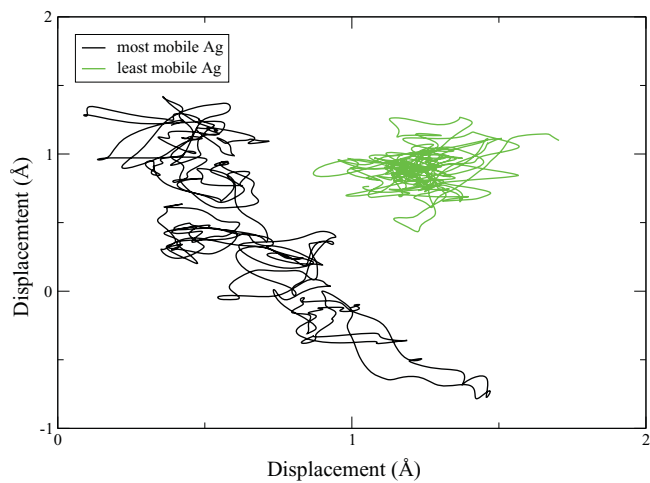


FIG. 16. (Color online) Trajectories of the most and the least diffusive Ag ions at 700 K as a function of time in amorphous $(\text{GeSe}_3)_{0.9}\text{Ag}_{0.1}$. Simulation time, 25 ps.

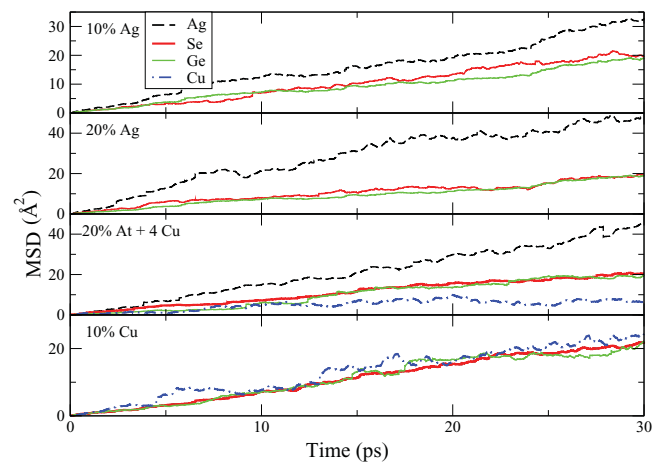


FIG. 19. (Color online) Mean square displacement of atoms in liquid $(\text{GeSe}_3)_{0.9}\text{Ag}_{0.1}$, $(\text{GeSe}_3)_{0.8}\text{Ag}_{0.2}$, $(\text{GeSe}_3)_{0.77}\text{Cu}_{0.03}\text{Ag}_{0.2}$, and $(\text{GeSe}_3)_{0.9}\text{Cu}_{0.1}$ (top to bottom, respectively) glasses at $T = 1000$ K. Ag (black line), Ge (green line), Se (red line), and Cu (blue).

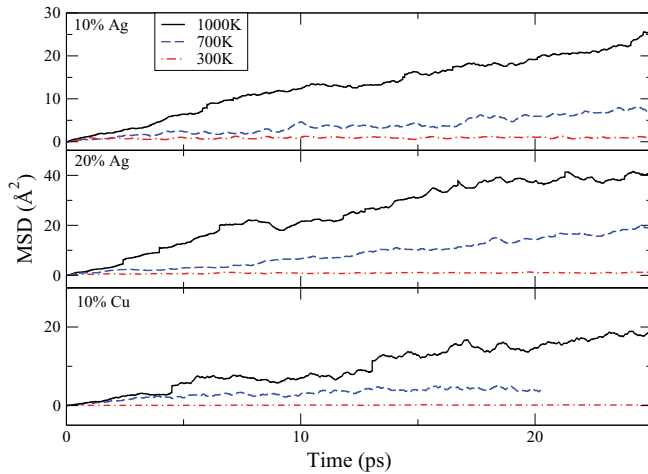


FIG. 20. (Color online) Temperature dependence of conductivity of ions for different models.

IV. CONCLUSION

We prepared different Ag- and Cu- doped GeSe_3 glass and liquid models by *ab initio* simulation using the “melt-quench” method and analyzed their structural and electronic properties. We also simulated dynamics of Ag and Cu ions using MD. We were able to reproduce structural data as provided by x-ray diffraction. From the EDOS we observed that an increase in

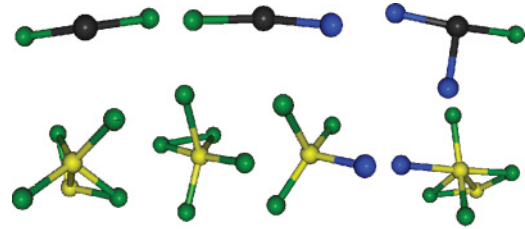


FIG. 21. (Color online) Local environments of Ag atoms (top) and Cu atoms (bottom). Black, green, blue, and yellow atoms represent, respectively, Ag, Se, Ge, and Cu.

Ag concentration widens the optical gap, whereas an increase in Cu concentration narrows the gap. We were also able to see the metallic behavior of the liquid systems with the gap closing completely at 1000 K. We were able to show the diffusion of the ions even on our time scale and predict the conductivity close to the experimental data. We also studied the trap and found that Cu traps are more rigid than those for Ag, making it very hard for Cu to diffuse.

ACKNOWLEDGMENTS

The authors want to thank Professor Gang Chen, Dr. Mingliang Zhang, and Bin Cai for their assistance and suggestions. This work was supported by NSF Grant No. DMR 09-03225.

*drabold@ohio.edu

¹M. Mitkova, in *Amorphous Semiconductors and Insulators*, edited by P. Boolchand (World Scientific, Singapore, 2000), p. 813.

²S. R. Ovshinsky, in *Non-Crystalline Materials for Optoelectronics*, edited by G. Lucovsky and M. Popescu (INOE, Bucharest, 2004), p. 1.

³R. Azoulay, H. Thibierge, and A. Brenac, *J. Non-Cryst. Solids* **18**, 33 (1975).

⁴M. Mitkova and M. N. Kozicki, *J. Non-Cryst. Solids* **299-302**, 1023 (2002).

⁵A. Piarristeguy, M. Mirandou, M. Fontana, and B. Arcondo, *J. Non-Cryst. Solids* **273**, 30 (2000).

⁶R. Dejus, S. Susman, K. Volin, D. Montague, and D. Price, *J. Non-Cryst. Solids* **143**, 162 (1992).

⁷G. Cuello, A. Piarristeguy, A. Fernández-Martínez, M. Fontana, and A. Pradel, *J. Non-Cryst. Solids* **353**, 729 (2007).

⁸D. N. Tafen, D. A. Drabold, and M. Mitkova, *Phys. Rev. B* **72**, 054206 (2005).

⁹I. Chaudhuri, F. Inam, and D. A. Drabold, *Phys. Rev. B* **79**, 100201(R) (2009); J. C. Phillips, *Rep. Prog. Phys.* **59** 1133 (1996).

¹⁰D. A. Drabold, *Eur. Phys. J. B.* **68**, 1 (2009).

¹¹G. Kresse and J. Furthmüller, *Phys. Rev. B* **54** 11169 (1996).

¹²J. M. Merino, S. Díaz-Moreno, G. Subías, M. León, *Thin Solid Films* **480-481**, 295 (2005).

¹³M. Mitkova, Y. Wang, and P. Boolchand, *Phys. Rev. Lett.* **83**, 3848 (1999).

¹⁴A. Piarristeguy, M. Fontana, and B. Arcondo, *J. Non-Cryst. Solids* **332**, 1 (2003).

¹⁵Mark Cobb, D. A. Drabold, and R. L. Cappelletti, *Phys. Rev. B* **54**, 12162 (1996).

¹⁶S. I. Simdyankin, S. R. Elliott, Z. Hajnal, T. A. Niehaus, and Th. Frauenheim, *Phys. Rev. B* **69**, 144202 (2004).

¹⁷M. Aniya and F. Shimojo, *J. Non-Cryst. Solids* **352**, 1510 (2006).

¹⁸David Chandler, in *Introduction to Modern Statistical Mechanics* (Oxford University Press, New York, 1987), pp. 249–250; N. W. Ashcroft and N. D. Mermin, in *Solid State Physics* (Harcourt, Orlando, FL, 1976), pp. 601–602; R. Kubo, *Rep. Prog. Phys.* **29**, 255 (1996).

¹⁹B. Arcondo, M. A. Ureña, A. Piarristeguy, A. Pradel, and M. Fontana, *Physica B* **389**, 77 (2007).

²⁰A. S. Kraemer and G. G. Naumis, *J. Chem. Phys.* **128**, 134516 (2008).